M. Wermuth, G. Gaias, S. D'amico
Safe Picosatellite Release from a Small Satellite Carrier
Journal of Spacecraft and Rockets, Vol. 52, N. 5, 2015, p. 1338-1347
doi:10.2514/1.A33036

Safe Picosatellite Release from a Small Satellite Carrier

Journal:	*Journal of Spacecraft and Rockets*
Manuscript ID:	2014-05-A33036.R3
Manuscript Type:	Full Paper
Date Submitted by the Author:	27-Apr-2015
Complete List of Authors:	Wermuth, Martin; DLR, GSOC Gaias, Gabriella; DLR, GSOC D'Amico, Simone; Stanford University, Aeronautics
Subject Index Category:	70500 Mission Design and Analysis < 70000 SPACE TECHNOLOGY, 33200 Spacecraft Dynamics < 30000 GUIDANCE, CONTROL, AND DYNAMICS TECHNOLOGY

AAS 14-414

SAFE PICOSATELLITE RELEASE FROM A SMALL SATELLITE CARRIER

Martin Wermuth,[*] Gabriella Gaias,[†] and Simone D'Amico[‡]

The Berlin InfraRed Optical System satellite, which is scheduled for launch in 2016, will carry onboard a picosatellite and release it through a spring mechanism. After separation, it will perform proximity maneuvers in formation with the picosatellite solely based on optical navigation. Therefore, it is necessary to keep the distance of the two spacecraft within certain boundaries. This is especially challenging, since the employed standard spring mechanism is designed to impart a separation velocity to the picosatellite. A maneuver strategy is developed in the framework of relative orbital elements. The goal is to prevent loss of formation while mitigating collision risk. The main design driver is the performance uncertainty of the release mechanism. The analyzed strategy consists of two maneuvers: the separation itself and a drift reduction maneuver of the Berlin InfraRed Optical System satellite after 1.5 revolutions. The selected maneuver parameters are validated in a Monte Carlo simulation. It is demonstrated that both the risk of formation evaporation (separation of more than 50 km), as well as the eventuality of a residual drift towards the carrier, are below 0.1%. In the latter case formation safety is guaranteed by a passive safety achieved through a proper relative eccentricity/inclination vector separation.

[*]Research Engineer, German Space Operations Center (GSOC/DLR), Oberpfaffenhofen , 82234 Wessling, Germany.
[†]Research Engineer, German Space Operations Center (GSOC/DLR), Oberpfaffenhofen , 82234 Wessling, Germany.
[‡]Assistant Professor, Department of Aeronautics & Astronautics, Stanford University, Durand Building, Stanford, CA 94305, USA.

NOTATION

a	semimajor axis of the carrier satellite [m]
ΔB	differential ballistic coefficient [m^2/kg]
$\Delta\bullet$	finite variation of a quantity
$\delta\bullet$	relative quantity
$\delta\boldsymbol{\alpha}$	nondimensional relative orbital elements ROE set
$\delta\mathbf{e}$	nondimensional relative eccentricity vector
$\delta\mathbf{i}$	nondimensional relative inclination vector
$\delta\lambda$	nondimensional relative longitude
δv_{R},δv_{T},δv_{N}	instantaneous velocity changes in local RTN frame [m/s]
e	eccentricity of the carrier satellite
e_i	delta-v error on the i-th tangential component [m/s]
ϵ_{xi}, ϵ_{yi}, ϵ_{zi}	simulated errors of the carrier attitude control during maneuver i [rad]
f_i	simulated performance factor of maneuver i
i	inclination of the carrier satellite [°]
φ	argument of latitude of the relative perigee [°]
k	odd natural number
n	mean angular motion of the carrier satellite [rad/s]
p	real number
ρ	atmospheric density [g/km^3]
θ	argument of latitude of the relative ascending node [°]
u	mean argument of latitude of the carrier satellite [°]
v	absolute value of velocity vector [m/s]
χ	function of the difference between the arguments of latitude of the two maneuvers
ω	argument of perigee of the carrier satellite [°]
Ω	right ascension of ascending node of the carrier satellite [°]
ξ	phase change of the relative eccentricity vector [rad]

INTRODUCTION

This paper addresses the design of a safe strategy to inject a picosatellite in low Earth orbit after separation from a small satellite carrier. The problem is motivated by the Autonomous Vision Approach Navigation and Target Identification (AVANTI) experiment onboard the Berlin InfraRed Optical System (BIROS [1]) spacecraft.

In the recent years, the deployment of small-scale satellites as secondary payloads into low Earth orbit has become more and more common [2, 3, 4, 5]. The miniaturization of technology and an increase in the number of educational scientific programs have both contributed to this trend. Within these applications, the launch vehicles are typically equipped with spring-based deployment devices which provide a linear velocity relative to the carrier that ranges from 0.3 to 2.0 m/s [6]. Since the main purpose of these technology demonstrations is focused on the ejected elements, the separation phase has to quickly and safely establish a certain relative distance, disregarding how different the final dynamics of the two vehicles are. Therefore, the ejection can simply be achieved by imparting the deployment delta-v in flight direction. In this case, the differential drag effect would increase the separation.

In 2010, in the frame of the Prototype Research Instruments and Space Mission technology Advancement (PRISMA [7]) mission, a different application scenario was successfully demonstrated in flight. It involved the separation of two satellites with the aim of performing some formation flying activities. The employed separation mechanism, a 3-point system with hooks and clamps kept in locked position by a single wire, was meant to provide a small delta-v (i.e., nominally 0.12 m/s [8]). Moreover, the accuracy of its true performance allowed considering safe relative orbits that intersect the local carrier horizon plane at an along-track separation of the order of 150 m. A further peculiarity of this satellite separation resided in the availability of a GPS-receiver on each satellite and of an inter-satellite link. Thus, the differential GPS relative navigation could be used to estimate both the deployment delta-v and the residual drift at the end of the separation phase [9].

The problem discussed in this paper presents commonalities with both mentioned categories of applications. On one hand, the BIROS spacecraft makes use of a spring-based Picosatellite Orbit Deployer (POD) device that provides a large and highly uncertain separation delta-v. On the other hand, the picosatellite release is relevant for the AVANTI experiment, where a noncooperative target (i.e., the ejected picosatellite, which has no onboard actuators for orbit control) is the target of several formation flying activities.

The major challenges of this application stem from the fact that a safe and stable relative motion of the formation has to be established shortly after separation subject to several operational constraints. Nevertheless, the results of this paper allow the extension and generalization of the relative eccentricity/inclination vector separation method [10] to a new class of distributed space systems. Overall this work proposes an effective way to solve a mission specific problem which might have relevant applications in future on-orbit servicing and distributed space systems architectures.

The proposed and analyzed guidance and maneuver planning approach is based on the relative eccentricity/inclination vector separation method which was first introduced by Harting et al. [11] for the collocation of geostationary satellites, later applied for long-range rendezvous in low Earth orbits by Montenbruck et al. [12] and finally extended to formation-flying [13] and on-orbit servicing scenarios [14]. Indeed a safe passively stable relative motion can be established after the release of a picosatellite from a satellite carrier by ensuring the (anti-) parallelism of the relative eccentricity and inclination vectors [12].

A further novelty of the proposed approach is the investigation, at a design level, of how additional relevant operational aspects impact the safety and the feasibility of the guidance plan. Specifically, this study addresses also the distance of the nearest transit of the picosatellite through the local along-track axis, the eventual delay and/or mis-execution of the drift-stopping maneuver performed by the carrier, and, finally, the achievement of a final relative drift with known and safe direction (i.e., which increases the along-track separation), regardless of the uncertainties in the whole control chain.

In order to deal with such a comprehensive scenario while establishing a desired passively safe stable relative orbit, the preliminary design of the maneuvering strategy is carried out in the Relative Orbital Elements (ROE) framework [15]. These parameters, in fact, are the integration constants of the Hill-Clohessy-Wiltshire equations and provide a direct insight into the geometry and thus into the safety characteristics of the relative motion. By making use of the simple relations between changes in ROE and applied delta-v derived from the inversion of the model of relative dynamics, a nominal scheme of maneuvers to accomplish the separation can be designed. Specifically it can be shown that a single maneuver cannot establish the parallelism of the relative eccentricity and inclination vectors, within the operational constraints of the application under consideration. On the contrary, a double maneuver strategy can accomplish this task through the tuning of parameters related to the mean along-track separation and to the size of the final relative orbit.

The ultimate validation of the preliminary designed guidance scheme is accomplished through multiple numerical analyses. These take into account several sources of uncertainty which affect the reliability of the nominal plan: 1) the POD delta-v magnitude error due to the spring release mechanism; 2) the BIROS attitude control error; 3) the BIROS maneuver execution error; and 4) the uncertainty in the knowledge of the differential ballistic coefficient. Considering all these uncertainties, a residual drift will remain after the second maneuver. The proposed strategy guarantees that the drift is in the desired direction irrespective of these uncertainties. Before the start of the AVANTI experiment, the residual drift is finally removed by a third maneuver which is planned on-ground after a dedicated orbit determination of the picosatellite.

In the following, first an overview of the mission with its requirements is provided. Secondly, the preliminary design of the guidance plan is described and a baseline scenario compliant with all the relevant operational aspects is selected. Finally, the results of nonlinear Monte Carlo (MC) simulations are presented and discussed, in the attempt to demonstrate the safety and efficiency of the overall methodology.

MISSION OVERVIEW AND REQUIREMENTS

Scheduled for launch in 2016, the BIROS satellite (60x80x80 cm, 140 kg) will be operated by the German Aerospace Center (DLR). Its primary task, next to several technology demonstration experiments (including AVANTI), will be the observation of wildfires in the frame of the FireBird mission. Together with the similar TET-1 satellite, which was launched in 2012 and is operated by DLR as well, it will form a loose constellation of Earth observation satellites. BIROS is designated for injection into an almost circular sun-synchronous orbit with a local time at the ascending node

(LTAN) of 9:30 am and an orbit height of 515 km. The spacecraft is equipped with a propulsion system and a fuel availability corresponding to circa 20 m/s of delta-v. Half of the fuel is allocated to the AVANTI experiment, while the other half is allocated to the primary mission objective.

The AVANTI experiment is intended to demonstrate vision-based, noncooperative autonomous approaches and recede operations of an active small satellite (BIROS) within separations between 10 km and 100 m from a picosatellite (10x10x10 cm, 1kg) making use of angles-only measurements. Reference [16] provides a description of the experiment objectives and design, whereas details about the onboard relative navigation filter are available in [17]. The picosatellite is originally carried by BIROS and later ejected through a POD deployer after the successful check-out and commissioning of all relevant BIROS subsystems. The AVANTI experiment is intended to start after the BIROS/Picosatellite formation has been brought to an initial safe configuration at about 5 km separation with minimal residual drift in along-track direction. This delicate operational task is solely ground-based and performed by the Flight Dynamics Services (FDS) division of the German Space Operations Center (GSOC), which is in charge of the orbit determination and control of the FireBird mission.

The mission profile is characterized by several external constraints which have to be considered during the analysis of a safe separation. First of all the separation must take place during a ground-station contact, which poses restrictions on the location of the deployment along the orbit and on the separation attitude for proper communication. In particular, the separation will take place at the beginning of a polar ground station contact and the argument of latitude u_1 for the separation is fixed to $88°$. Since a standard POD is adopted, the size of the delta-v imparted to the picosatellite at ejection is 1.41 m/s with a basically unknown dispersion. If oriented in along-track direction, this corresponds to about 2.8 km semi-major axis difference between the BIROS and picosatellite orbits, which produces an along-track drift of 27 km/orbit or 405 km/day. Since during this phase, the only means of navigation information for the picosatellite is radar tracking from ground, with associated latencies of typically 24 hours, the risk of formation evaporation would be too high when adopting this conventional separation strategy. In this study, we assume that a mean along-track separation larger than 50 km corresponds to an evaporated formation. This value is derived from the in-flight experience of noncooperative far-range approaches gained by the DLR/GSOC formation reacquisition experiment accomplished in 2011 at the end of the nominal phase of the PRISMA mission [18]. At that time, an inter-satellite separation of 55 km was recovered in one week mainly based on two-line-elements information. Nevertheless, due to all the uncertainties that characterize the separation event and control chain, a certain residual drift towards evaporation remains also when employing the guidance scheme proposed here. The radar tracking facility foreseen within the FireBird mission is the imaging radar (TIRA) station in Germany [19]. According to it, due to the different sizes of the BIROS satellite and the picosatellite, a minimum distance of 5 km is required for TIRA to be able to distinguish the signal from the two spacecraft. Typically two tracking passes with a spacing of 12 hours are necessary for an accurate orbit determination.

Additional geometrical constraints are introduced by the camera employed by the AVANTI experiment. The experience from previous missions suggests that the camera should be able to detect the picosatellite up to a distance of 10 km [20]. The separation scenario must ensure the visibility of the picosatellite at the start of the AVANTI experiment, considering that the half field of view of the camera is $6.8°$ horizontally and $9.15°$ vertically.

RELATIVE MOTION DESCRIPTION

The relative motion is parameterized by this set of dimensionless relative orbital elements (ROE):

$$\delta\boldsymbol{\alpha} = \begin{pmatrix} \delta a \\ \delta\lambda \\ \delta e_x \\ \delta e_y \\ \delta i_x \\ \delta i_y \end{pmatrix} = \begin{pmatrix} \delta a \\ \delta\lambda \\ \delta e\cos\varphi \\ \delta e\sin\varphi \\ \delta i\cos\theta \\ \delta i\sin\theta \end{pmatrix} = \begin{pmatrix} (a-a_\mathrm{d})/a_\mathrm{d} \\ u-u_\mathrm{d}+(\Omega-\Omega_\mathrm{d})\cos i_\mathrm{d} \\ e\cos\omega - e_\mathrm{d}\cos\omega_\mathrm{d} \\ e\sin\omega - e_\mathrm{d}\sin\omega_\mathrm{d} \\ i-i_\mathrm{d} \\ (\Omega-\Omega_\mathrm{d})\sin i_\mathrm{d} \end{pmatrix} \tag{1}$$

where a, e, i, Ω, and M denote the classical Keplerian elements and $u = M + \omega$ is the mean argument of latitude. The subscript "d" labels the deputy spacecraft of the formation, which plays the role of the maneuverable carrier satellite (BIROS) and defines the origin of the local radial-tangential-normal (RTN) frame. The quantities $\delta\mathbf{e} = (\delta e \cos\varphi, \delta e \sin\varphi)^{\mathrm{T}}$ and $\delta\mathbf{i} = (\delta i \cos\theta, \delta i \sin\theta)^{\mathrm{T}}$ define the dimensionless relative eccentricity and inclination vectors, where φ and θ respectively represent the perigee and ascending node of the relative orbit [12]. In the following, their magnitudes are shortly quoted as $\delta e = \|\delta\mathbf{e}\|$ and $\delta i = \|\delta\mathbf{i}\|$, whereas the subscript is dropped, meaning that all the absolute orbital quantities appearing in the equations belong to the carrier satellite.

Under the assumptions of the Hill-Clohessy-Wiltshire equations (HCW, [21]) the quantities $a\delta e$ and $a\delta i$ provide the amplitudes of the in-plane and out-of-plane relative motion oscillations (see Figure 1), whereas relative semi-major axis, $a\delta a$, and relative mean longitude, $a\delta\lambda = a(\delta u + \delta i_y \cot i)$, provide mean offsets in radial and along-track directions respectively [10, 22]. Moreover, if no orbital perturbations are considered, the only ROE that varies with time is the relative mean longitude according to:

$$\delta\lambda(u) = -1.5(u - u_0)\delta a_0 + \delta\lambda_0 \tag{2}$$

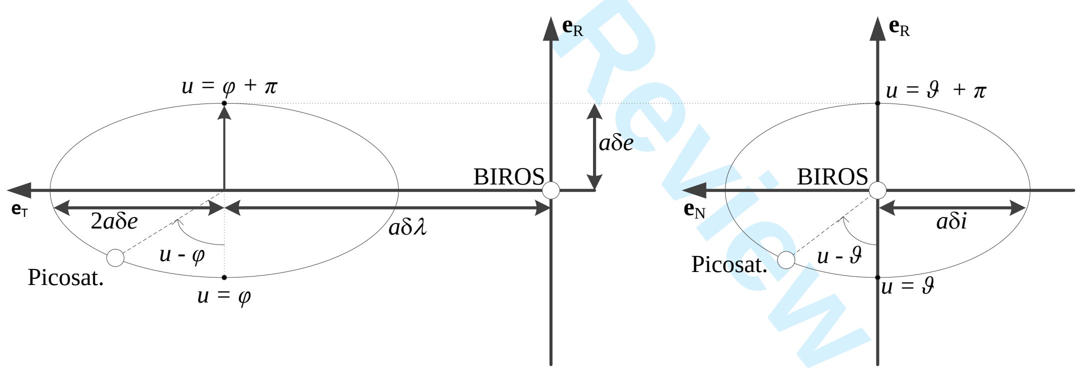

Figure 1. Sketch of Relative Orbit Elements (ROE) and their relation to the relative motion in the RTN frame.

According to the model of the relative dynamics just introduced, the instantaneous dimensional variations of the ROE caused by an impulsive maneuver (or an instantaneous velocity change) at the mean argument of latitude u_M are given by:

$$\begin{array}{lllll} a\Delta\delta a & = & & +2\delta v_\mathrm{T}/n & \\ a\Delta\delta\lambda & = & -2\delta v_\mathrm{R}/n & & \\ a\Delta\delta e_x & = & +(\delta v_\mathrm{R}/n)\sin u_\mathrm{M} & +2(\delta v_\mathrm{T}/n)\cos u_\mathrm{M} & \\ a\Delta\delta e_y & = & -(\delta v_\mathrm{R}/n)\cos u_\mathrm{M} & +2(\delta v_\mathrm{T}/n)\sin u_\mathrm{M} & \\ a\Delta\delta i_x & = & & & +(\delta v_\mathrm{N}/n)\cos u_\mathrm{M} \\ a\Delta\delta i_y & = & & & +(\delta v_\mathrm{N}/n)\sin u_\mathrm{M} \end{array} \tag{3}$$

which, as explained in [22], can be equivalently derived either from the Gauss Variational Equations or from the HCW solution at the time when $u = u_\mathrm{M}$. In Eq. (3), n indicates the mean motion of the carrier and the delta-v is expressed in the RTN frame:

$$\delta \mathbf{v} = (\delta v_\mathrm{R}, \delta v_\mathrm{T}, \delta v_\mathrm{N})^\mathrm{T} \tag{4}$$

Before the release of the picosatellite, the relative state $a\delta\boldsymbol{\alpha}$ is null. Then, if a single separation maneuver is executed at the mean argument of latitude u_1, the following ROE variations can be established at $u = u_1$:

$$\left\{ \begin{array}{rcl} na\Delta\delta a & = & 2\delta v_\mathrm{T} \\ na\Delta\delta\lambda & = & -2\delta v_\mathrm{R} \\ na\Delta\delta e & = & \sqrt{\delta v_\mathrm{R}^2 + 4\delta v_\mathrm{T}^2} \\ \tan(u_1 - \xi) & = & \dfrac{\delta v_\mathrm{R}}{2\delta v_\mathrm{T}} \\ na\Delta\delta i & = & |\delta v_\mathrm{N}| \\ \tan(u_1) & = & \dfrac{\Delta\delta i_y}{\Delta\delta i_x} \end{array} \right. \tag{5}$$

where ξ denotes the obtained phase angle of the relative eccentricity vector.

As mentioned above, the location of the first separation maneuver is fixed by the need of performing it during a given ground contact. Furthermore, the magnitude is fixed by making use of a POD device with a fixed δv of 1.41 m/s. On the other hand, the direction of the impulse is freely selectable.

This poses the following constraint on the magnitude of the separation maneuver:

$$\delta v = \|\delta \mathbf{v}\| = \sqrt{\delta v_{\mathrm{R}}^2 + \delta v_{\mathrm{T}}^2 + \delta v_{\mathrm{N}}^2} \tag{6}$$

and the number of effective degrees of freedom of the problem is reduced so that one can satisfy only two of the conditions of Eq. (5).

By analyzing the obtainable relative motion within the requirements of this application scenario, it can be proven that if $\delta v_{\mathrm{T}} = 0$, the established relative motion is characterized by $\delta \mathbf{e}^{\mathrm{T}} \delta \mathbf{i} = 0$ [see Eq. (3)]. In other words, radial and cross-track maneuvers at the same location produce perpendicular relative eccentricity and inclination vectors. Thus the minimum separation in the R–N plane is null, which is not acceptable for safety reasons in the presence of along-track position uncertainties [13]. In contrast, if $\delta v_{\mathrm{T}} \neq 0$ and $\delta v_{\mathrm{R}} \neq 0$, the phase of $\delta \mathbf{e}$ can be changed. Unfortunately this change is not as much needed to obtain (anti-) parallel relative eccentricity/inclination vectors after one maneuver.

It is emphasized that, in order to avoid a collision, it is necessary to establish a certain drift in the relative motion through the first separation maneuver (i.e., δv_{T} must be $\neq 0$). In this case, in fact, the first passage of the deputy satellite across the along-track axis will occur after some separation is built up.

In conclusion, since it is not possible to achieve a bounded passively safe orbit through a single separation maneuver, a second maneuver is strictly required, as addressed in the following section.

Separation preliminary design: the double-maneuver scheme

The analytical form of the general expression of the in-plane double-pulse maneuvers' scheme, for whatever aimed final conditions, as a function of the mean arguments of latitude of the two maneuvers is given in [15] [i.e., Eq.(12)]. Nevertheless, this expression is quite complicated and does not allow an immediate geometrical insight into the geometry of the relative motion. At a preliminary stage, Eq.(2.42) of [10] can be used:

$$\begin{aligned}
\delta v_{\mathrm{R1}} &= \tfrac{na}{2}\left(-\tfrac{\Delta\delta\lambda^*}{2} + \Delta\delta e \sin(u_1-\xi) \right) - \tfrac{na}{2}\chi\left(\Delta\delta a - \Delta\delta e \cos(u_1-\xi) \right)\\
\delta v_{\mathrm{T1}} &= \tfrac{na}{4}\left(+\Delta\delta a + \Delta\delta e \cos(u_1-\xi) \right) - \tfrac{na}{4}\chi\left(\tfrac{\Delta\delta\lambda^*}{2} + \Delta\delta e \sin(u_1-\xi) \right)\\
\delta v_{\mathrm{R2}} &= \tfrac{na}{2}\left(-\tfrac{\Delta\delta\lambda^*}{2} - \Delta\delta e \sin(u_1-\xi) \right) + \tfrac{na}{2}\chi\left(\Delta\delta a - \Delta\delta e \cos(u_1-\xi) \right)\\
\delta v_{\mathrm{T2}} &= \tfrac{na}{4}\left(+\Delta\delta a - \Delta\delta e \cos(u_1-\xi) \right) + \tfrac{na}{2}\chi\left(\tfrac{\Delta\delta\lambda^*}{2} + \Delta\delta e \sin(u_1-\xi) \right)
\end{aligned} \tag{7}$$

with

$$\chi = \frac{\sin\Delta u}{\cos\Delta u - 1} \qquad \Delta u = u_2 - u_1 \qquad \xi = \arctan\left(\frac{\Delta\delta e_y}{\Delta\delta e_x}\right) \tag{8}$$

Equation (7) provides an analytical expression of the double-impulse in-plane scheme to achieve a prescribed total variation of $\Delta\delta a$, $\Delta\delta\mathbf{e}$, and $\Delta\delta\lambda^*$. This expression is very useful since in our application the initial relative state is null, and the total aimed variation coincides with the final aimed relative state:

$$\Delta\delta\bullet = \delta\bullet_{\mathrm{F}} \qquad \text{and} \qquad \varphi_{\mathrm{F}} = \xi \tag{9}$$

The simple and practical form of Eq. (7) has been obtained by neglecting that $\delta\lambda$ changes over time when the relative semi-major axis after the first maneuver δa_1 is not null, according to Eq. (2). Therefore the truly obtainable relative longitude at the final time $\delta\lambda_{\mathrm{F}} = \Delta\delta\lambda$ will not exactly amount to $\Delta\delta\lambda^*$. The required correction is later on discussed through Eq. (14). Nevertheless, at a preliminary design stage, Eq. (7) is acceptable and allows achieving a much simpler expression of the in-plane delta-vs.

When dealing with the in-orbit release of a satellite, Eq. (7) must be complemented with the out-of-plane equations. The passive safety constraint of final (anti)parallelism of the relative eccentricity/inclination vectors, in fact, couples back to the impulsive reconfiguration problem.

In the following, the remaining specific requirements of the separation problem are listed and discussed, together with their geometrical interpretation in the ROE space. In Figure 2 all the final desired quantities, which are the parameters that appear in Eq. (7) are marked in black. The other quantities represent the intermediate values obtained during the execution of a double-impulse maneuvering scheme.

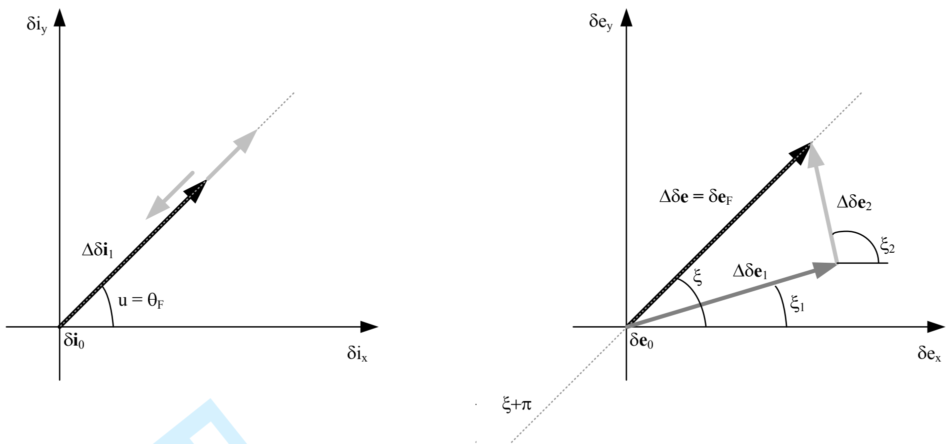

(a) Relative inclination plane (b) Relative eccentricity plane

Figure 2. Sketch in the ROE space of the maneuvering scheme of Eq. (7) **to achieve passive safety**

The following features characterize this application scenario. First of all, the location of the first maneuver u_1 is fixed and known, since the deployment has to occur during the aforementioned ground contact. Consequently, the phase of the relative inclination vector after the first maneuver θ is also fixed. This is shown in Figure 2 by the dotted light gray segment in the $\delta \mathbf{i}$ plane. Note that $u = u_1 = \theta_{\mathrm{F}}$, assuming that $\delta v_{\mathrm{N}1} > 0$ without loss of generality. Furthermore in order to achieve passive safety, it has to be imposed that the phase of the final $\delta \mathbf{e}$, ξ is equal to θ_{F}. This is shown in Figure 2 by the dotted light gray segment in the first and third quadrants of the $\delta \mathbf{e}$ plane. Thus, in a general case, one can impose $\xi = \theta_{\mathrm{F}} + \eta$, where the service parameter η can only assume the values of 0 or π. The aim is to establish a final stable relative orbit, thus $\delta a_{\mathrm{F}} = 0$. This implies that all terms in $\Delta\delta a$ in Eq. (7) vanish. Equation (7) is defined for $\Delta u \neq 0$ or $\neq 2\pi$. In all other cases, χ weights the effect of the maneuvers' spacing on the final four in-plane delta-v expressions. In the special case of k odd number and $\Delta u = k\pi$ the second part of Eq. (7) vanishes. As a result the delta-v expressions are characterized by a symmetrical form. Moreover, in these particular locations of the second maneuver, the effect of the second out-of-plane maneuver can only change the magnitude of δi, and not the phase θ_{F}, whenever $\delta v_{\mathrm{N}2}$ is nonzero. This is marked by the gray arrows in the left side of Figure 2. As already mentioned above, the first maneuver is accomplished by the deployment device, thus its magnitude is constrained to δv. This introduces a relationship on the three RTN components, and, consequently on the achievable $\Delta\delta e$, $\Delta\delta\lambda^*$, and $\Delta\delta i$.

By taking into account the aforementioned requirements, the delta-v expressions of Eq. (7) simplify to:

$$\begin{aligned} \delta v_{\mathrm{R1}} &= -\tfrac{na}{4}\left(\Delta\delta\lambda^* \right) \\ \delta v_{\mathrm{T1}} &= \pm\tfrac{na}{4}\left(\Delta\delta e \right) \\ \delta v_{\mathrm{R2}} &= -\tfrac{na}{4}\left(\Delta\delta\lambda^* \right) \\ \delta v_{\mathrm{T2}} &= \mp\tfrac{na}{4}\left(\Delta\delta e \right) \end{aligned} \tag{10}$$

since $u_1 = \xi$. The signs of Eq. (10) are determined by fixing η (i.e., the final $\delta\mathbf{e}/\delta\mathbf{i}$ configuration) and by the sign of $\Delta\delta\lambda^*$, which is equivalent to the sign of $\delta\lambda_{\mathrm{F}}$ (i.e., picosatellite leading or following the carrier).

At conclusion of this preliminary design section, the simple delta-vs expression of Eq. (10) has been achieved. This is the result of imposing the satisfaction of the separation final conditions (i.e., passively safe bounded relative orbit) through only two maneuvers. Moreover, the operational requirement on the location of the picosatellite ejection has been included, together with the two design assumptions of $\delta v_{\mathrm{N1}} > 0$ and $\chi = 0$. At this point, the remaining degrees of freedom of the separation problem are two among δe_{F}, δi_{F} and $\delta\lambda_{\mathrm{F}}$ together with the spacing between the maneuvers (i.e., the number of half revolutions k). These parameters are fixed as soon as an aimed final orbit is identified. Therefore, the next section deals with the identification of such a nominal baseline, in order to cope with some operative aspects of crucial importance in realistic scenarios.

Baseline identification in compliance with the operative constraints

This section discusses how some operative constraints impact the degrees of freedom of the preliminary design formulation. Outcome is the identification of feasible baselines for the aimed relative orbit. An analysis and verification of their robustness with respect to system uncertainties is accomplished afterwards.

Table 1 lists the main operative constraints that are involved in the in-orbit release of a satellite, as explained above. Constraints safety #1 and visibility #1 determine the domain of the aimed relative mean longitude, that is the mean satellite separation in tangential direction. Safety constraint #2

Table 1. Meaningful operative constraints for the in-orbit satellite release

Constraint	Identifier	Description	Consequence
safety	1	TIRA tracking capability	$\lvert a\delta\lambda_{\mathrm{F}}\rvert \geq 5000$ m
safety	2	1st cross of the along-track axis	Given $\delta\lambda_{\mathrm{F}}$ and $\chi = 0$, fixes η
safety	3	Effect of differential drag	Choice of the direction of $\delta\lambda_{\mathrm{F}}$
safety	4	Delay of 2nd maneuver	No collision before passive safety achievement
safety	5	Passive safety	Given η, minimum size of δe_{F} and δi_{F}
safety	6	Sign of δa after 1st maneuver	$\lvert\delta v_{\mathrm{T1}}\rvert$ greater than spring error
safety	7	Truly obtainable $a\delta i$	aimed $\delta i > (\delta i_{\mathrm{min}} + \text{margin})$
visibility	1	Picosat camera detectability	$\lvert a\delta\lambda_{\mathrm{F}}\rvert \leq 10000$ m
visibility	2	Camera FOV in R direction	$a\delta e_{\mathrm{max}} < 596$ m at $a\delta\lambda_{\mathrm{F}} = 5000$ m
visibility	3	Camera FOV in N direction	$a\delta i_{\mathrm{max}} < 805$ m at $a\delta\lambda_{\mathrm{F}} = 5000$ m

determines the parallel or anti-parallel $\delta\mathbf{e}/\delta\mathbf{i}$ configuration (i.e., η). In particular, if the picosatellite is released so that at the end of the separation it leads the carrier in flight direction, an instantaneous negative radial delta-v must be imparted (i.e., $\delta v_{\mathrm{R1}} < 0$). Therefore, in order to avoid an immediate crossing of the local along-track axis, the semi-major axis of the picosatellite shall be reduced (i.e., $\delta v_{\mathrm{T1}} < 0$) to drift towards positive along-track separations. This combination of signs in Eq. (10) is obtained with $\eta = \pi$ in Eq. (7), since $\xi = \theta_{\mathrm{F}} + \eta$. Thus the final aimed relative orbit must have anti-parallel relative e/i vectors.

The safe complementary situation (i.e., picosatellite released to follow the carrier) requires $\delta v_{\mathrm{R1}} > 0$ and a positive drift (i.e., $\delta v_{\mathrm{T1}} > 0$). According to the chosen maneuvering scheme, this is obtained if $\eta = 0$, thus by establishing a parallel configuration.

The choice of having picosatellite leading/following BIROS can be taken by considering the safety constraints #3 and #4. They address the natural effect of the differential drag. In this application, the ballistic drag coefficient of the picosatellite is greater than that of BIROS, thus its orbit lowers faster, producing a drift at a relative level (note that in this paper the ballistic drag coefficient $B = C_D A/m$ is used instead of its inverse quantity the ballistic coefficient, in order to be in line with other satellite work). Specifically, if the picosatellite is leading the carrier in flight direction, the natural drift tends towards larger separations. On the opposite situation, the picosatellite will tend to come back towards the carrier. The trade-off between *evaporation* or *proximity* shall take into account the constraint safety #4 as well. According to it, any dangerous situation before the accomplishment of the second maneuver shall be avoided. This is motivated by the fact that a single maneuver is not able to establish passive safety (see previous sections).

Therefore, in order to satisfy the first four safety requirements, according to this scenario, a final configuration with the picosatellite leading the carrier in positive tangential direction is to be preferred. Consequently, $\Delta\lambda_{\mathrm{F}} > 0$ and $\eta = \pi$. The range of feasible sizes of the aimed relative orbit are derived from the remaining constraints of Table 1.

Constraint safety #6 requires that the direction of the drift is unequivocally defined, disregarding the size of execution error of the first maneuver. Thus, by considering an error $\tilde{e}$ of magnitude 0.141 m/s (i.e., 10% of the total magnitude δv), the delta-v in tangential direction must produce a negative drift in any case. This implies:

$$|\delta v_{\mathrm{T1}}| = \frac{na}{4}\delta e_{\mathrm{F}} > \tilde{e} \quad \rightarrow \quad a\delta e_{\mathrm{min}} = 511.25\,\mathrm{m} \tag{11}$$

for the carrier at an an orbit altitude of 515 km.

The same error consideration applied in the normal component of the delta-v impacts the truly obtainable magnitude of the relative inclination vector. This is referred as constraint safety #7 in Table 1, and fixes the margin equal to $\tilde{e}/n$ [i.e., 127.81 m at the same orbit height of Eq. (11)], being n the carrier mean motion.

The minimum size of the stable final relative orbit is also limited by passive safety considerations (i.e., constraint safety #5), that ask for a minimum R–N distance of $100 - 150$ m. By merging all these requirements, the lower bounds reported in Table 2 are obtained.

Finally, the maximum size of the relative orbit is constrained by the Field Of View (FOV) of the camera (i.e., visibility constraints #2 and #3). The worst case scenario occurs at the minimum allowed mean relative longitude value (i.e., $a\delta\lambda_{\mathrm{F}} = 5000$ m). By making use of Eq. (3) [20], and by neglecting the correction due to curvature, the following limits are identified:

$$\delta e_{\mathrm{F}} < \tan(6.8°)|\delta\lambda_{\mathrm{F}}| \qquad\qquad \delta i_{\mathrm{F}} < \tan(9.15°)|\delta\lambda_{\mathrm{F}}| \tag{12}$$

and the subsequent values are also collected in Table 2.

Table 2. Admissible sizes of the final relative orbit

Aimed ROE	Min magnitude [m]	Max magnitude [m]
$a\delta\lambda$	5000	10000
$a\delta e$	512	596
$a\delta i$	278	805

It is emphasized that the three final magnitudes $\delta\lambda$, δe, and δi cannot be chosen independently, due to the constraint on the magnitude of the first maneuver. Moreover, in Eq. (10) the $\Delta\delta\lambda^*$ value appears instead of the true $\delta\lambda_{\mathrm{F}}$, due to the simplifications introduced by Eq. (7).

Both these points suggest choosing δe and δi as design parameters, in their domains of feasibility. Consequently, the value of the radial component of the first delta-v is given by:

$$\delta v_{\mathrm{R1}} = -\sqrt{\delta v^2 - \delta v_{\mathrm{T1}}{}^2 - \delta v_{\mathrm{N1}}{}^2} \tag{13}$$

and $\Delta\delta\lambda^*$ is then computed using the first of Eq. (10).

This obtained value influences the choice of k, so that the final $\delta\lambda_{\mathrm{F}}$ is in its domain of feasibility. The relationship between the obtained relative mean longitude and $\Delta\delta\lambda^*$ of Eq. (7) is provided by:

$$\delta\lambda_{\mathrm{F}} = -1.5(k\pi)\delta a_1 + \Delta\delta\lambda^* \tag{14}$$

where $\delta a_1 = (2/n)\delta v_{\mathrm{T1}}$. Therefore, once fixed δv_{R1} (i.e., fixed δe and δi), k can be chosen as the odd natural number comprised in:

$$-\frac{5000 - \Delta\delta\lambda^*}{1.5\pi\delta a_1} \leq k \leq -\frac{10000 - \Delta\delta\lambda^*}{1.5\pi\delta a_1} \tag{15}$$

Some remarks can be added when dealing with the final selection of the baseline (i.e., aimed δe and δi). Visibility constraints #2 and #3 can be handled as *soft* constraints, since they become less critical when the separation increases. Both differential drag and the choice of a bigger k contribute to this. The magnitude of δi can be small (coherently with its domain) in order to avoid further consumption of delta-v due to a second cross-track burn. Moreover, this allows allocating more delta-v to the tangential and radial components of the first maneuver, which is fruitful for safety constraint #6 and for establishing faster a certain separation. Visibility constraints #1 could also be softened since later corrections can be accomplished before switching to visual-based relative navigation (at the cost of further delta-v consumption).

An example of feasible baseline can be obtained by choosing the following values:

$$\begin{aligned} a\delta e_{\mathrm{F}} &= 590\,\mathrm{m} \\ a\delta i_{\mathrm{F}} &= 400\,\mathrm{m} \end{aligned} \tag{16}$$

leading to these nominal delta-v magnitudes:

$$\begin{aligned} \delta\mathbf{v}_1 &= (\delta v_{\mathrm{R1}}, \delta v_{\mathrm{T1}}, \delta v_{\mathrm{N1}})^{\mathrm{T}} = (-1.329250, -0.162718, 0.441269)^{\mathrm{T}}\ \mathrm{m/s} \\ \delta\mathbf{v}_2 &= (\delta v_{\mathrm{R2}}, \delta v_{\mathrm{T2}}, \delta v_{\mathrm{N2}})^{\mathrm{T}} = (-1.329250, +0.162718, 0.0)^{\mathrm{T}}\ \mathrm{m/s} \end{aligned} \tag{17}$$

The admissible values of k to satisfy Eq. (15) are $[1, 3]$. It is emphasized that, since the delta-vs do not depend on this choice [see Eq. (10)], the same delta-v plan remains valid in the case that any anomaly prevented executing the second maneuver. Besides, a delay in the execution of such maneuver causes the aimed $\delta\lambda_{\mathrm{F}}$ to increase according to Eq. (14).

Figure 3 shows the nominal relative trajectory obtained with $k = 3$ in the RTN frame with the BIROS satellite in the origin. At this level of the analysis no disturbances are included in the ROE propagation. The thin lines in the R–N, R–T, and N–T views define the area of the FOV of the camera mounted on the BIROS spacecraft, while the solid gray line denotes the relative trajectory prior to the second maneuver and the solid black line denotes the relative trajectory after the second maneuver.

Before dealing with the verification of the chosen baseline with respect to system's uncertainties, a final design problem needs to be addressed. It concerns the sign of the final relative drift when the executed delta-vs differ from the nominal commanded ones. This topic is relevant since one cannot estimate the truly executed first impulse before accomplishing the second maneuver.

Being the drift linked to the tangential components of the delta-vs, at a design level it can be assumed that no error is accomplished on the radial and normal components of Eq. (17). When the

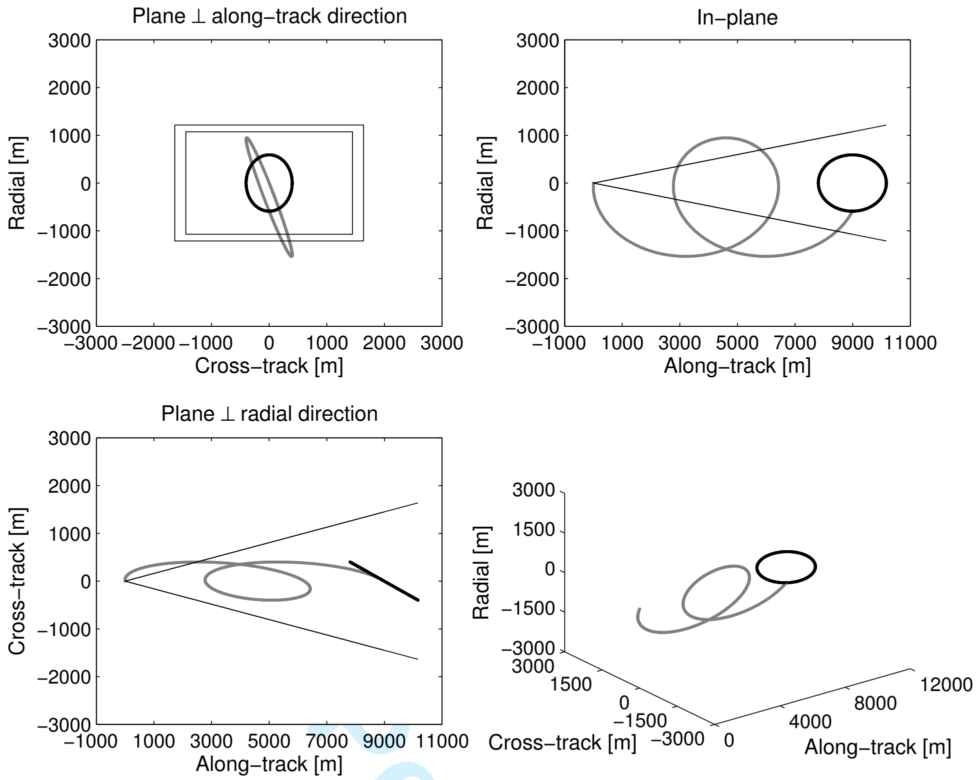

Figure 3. Example of the feasible baseline of Eq. (16) **with delta-vs of Eq.** (17)

truly executed first tangential maneuver is given by:

$$\delta v_{\mathrm{T1}}^{*} = \delta v_{\mathrm{T1}} + e_1 \tag{18}$$

a possible critical situation can arise if e_1 reduces the magnitude of $\delta v_{\mathrm{T1}}^{*}$ (i.e., $e_1 > 0$). In this case, the second tangential maneuver would produce a drift reversal resulting in a drift of the picosatellite towards the carrier. Since the delta-v values are computed according to Eq. (10), increasing the baseline value of $\Delta\delta e$ does not remove this problem.

A mitigation of this issue can be achieved by commanding the following nominal tangential delta-v for the second maneuver instead:

$$\delta v_{\mathrm{T2}}^{*} = \delta v_{\mathrm{T2}} + e_2 - |p| \tag{19}$$

where the parameter p has to be sized in order to properly determine the strength of the drift reduction. The error in the tangential component of the second maneuver e_2 increases the magnitude of the drift reduction whenever $e_2 > 0$.

This approach exploits the particular structure of this separation design formulation. It can be shown, in fact, that given the two maneuvers spaced by $k\pi$ and having $|\delta v_{\mathrm{R1}}| = |\delta v_{\mathrm{R2}}|$ [see Eq. (10)], the final phase of the relative eccentricity vector ξ remains the same whatever value of δv^*_{T1} and δv^*_{T2} are performed. Moreover, the final magnitude of the relative eccentricity vector is given by:

$$a\delta e^*_{\mathrm{F}} = \frac{1}{n}\sqrt{4(\delta v^{*\,2}_{\mathrm{T1}} + \delta v^{*\,2}_{\mathrm{T2}} - 2\delta v^*_{\mathrm{T1}}\delta v^*_{\mathrm{T2}})} \tag{20}$$

Hence, the parameter p can be chosen such that the sign of the final relative semi-major axis δa^*_{F} is negative even with the greatest under performance of the POD device. At the same time, p is limited by the need to perform at least some drift reduction. These two statements can be formalized as:

$$\begin{cases} \delta v_{\mathrm{T2}} - e_2 - |p| > 0 & \rightarrow \quad \delta v^*_{\mathrm{T2}} > 0 \\ \delta v_{\mathrm{T2}} + e_2 - |p| \leq |\delta v_{\mathrm{T1}}| - e_1 & \rightarrow \quad \delta a^*_{\mathrm{F}} < 0 \end{cases} \tag{21}$$

which lead to the following design range for p:

$$e_1 + e_2 \leq |p| < \frac{na}{4}\delta e_{\mathrm{F}} - e_2 \tag{22}$$

having used $\delta v_{\mathrm{T2}} = |\delta v_{\mathrm{T1}}| = na\delta e_{\mathrm{F}}/4$.

To conclude this section, the choice of the aimed final relative orbit shall be accomplished by selecting the values $(a\delta e_{\mathrm{F}}, a\delta i_{\mathrm{F}}, p)$ that allows satisfying all the constraints considered so far. Moreover one should verify that the final $a\delta e^*_{\mathrm{F}}$ from Eq. (20) meets the passive safety requirement (i.e., safety constraint #5 in Table 1), despite the presence of p. Finally, the case of over performance of the POD device shall be taken into account. The maximum drift imparted by the first maneuver shall not bring to evaporation, having weakened the drift reduction through p.

MONTE CARLO SIMULATION

In order to validate the risk of the planned maneuver strategy, Monte Carlo (MC) simulations have been performed in the ROE framework. It should be noted that all simulation runs were executed generating 100000 samples but only 1000 are plotted for readability.

The simulation uses the dispersion parameters discussed below. The uncertainty of the POD mechanism is unknown, hence a pessimistic dispersion with a standard deviation of 10% of the overall delta-v is assumed. This is expressed by multiplying the first maneuver by a factor f_1, which has a mean value of 1 and a standard deviation of 0.1. The execution accuracy of the BIROS propulsion system is unknown at this stage. Similarly to the POD mechanism, a dispersion of 5% is assumed. This is expressed by multiplying the second maneuver by a factor f_2, which has a mean value of 1 and a standard deviation of 0.05. It is noted that it will be possible to accurately calibrate the BIROS thrusters during the commissioning phase, hence this value might change at a later stage. The BIROS satellite is known to have an attitude control accuracy of 30 arcsec. This is expressed by multiplying both maneuvers by a rotation matrix for infinitesimal angles, where the quantities ϵ_x, ϵ_y and ϵ_z have a mean value of 0 and a standard deviation of 30". The simulated delta-vs $\delta v^{\mathrm{s}}_{\mathrm{R}i}$ for maneuvers $i = 1, 2$ are obtained by:

$$\begin{pmatrix} \delta v^{\mathrm{s}}_{\mathrm{R}i} \\ \delta v^{\mathrm{s}}_{\mathrm{T}i} \\ \delta v^{\mathrm{s}}_{\mathrm{N}i} \end{pmatrix} = f_i \begin{pmatrix} 1 & \epsilon_{zi} & -\epsilon_{yi} \\ -\epsilon_{zi} & 1 & \epsilon_{xi} \\ \epsilon_{yi} & -\epsilon_{xi} & 1 \end{pmatrix} \begin{pmatrix} \delta v_{\mathrm{R}i} \\ \delta v_{\mathrm{T}i} \\ \delta v_{\mathrm{N}i} \end{pmatrix} \tag{23}$$

The effect of the differential drag on the relative mean longitude and relative semi-major axis can be computed as [10]:

$$a\delta\lambda(t) = \frac{3}{4n^2}\Delta B \rho v^2 \left(u(t) - u_0\right)^2 \tag{24}$$

$$a\delta a(t) = -\frac{1}{n^2}\Delta B \rho v^2 \left(u(t) - u_0\right) \tag{25}$$

Considering the physical properties of BIROS (cross-section of 0.8 m $\times$ 0.6 m at nominal attitude, weight of 140 kg) and the picosatellite (cross-section of 0.1 m $\times$ 0.1 m, weight of 1 kg) with an assumed atmospheric density of $\rho = 1\mathrm{g/km}^3$ and a drag-coefficient of $c_d = 2.3$, the relative ballistic drag coefficient can be determined as $\Delta B = 0.0151\ \mathrm{m}^2/\mathrm{kg}$. Nevertheless the atmospheric density, the true effective cross-section (due to attitude maneuvers) and the true weight of the satellites (e.g. due to fuel consumption) are difficult to predict. Hence an ad-hoc uncertainty of the differential drag with standard deviation of 20% is applied in the Monte Carlo simulations.

Using the baseline maneuvers determined above [see Eq. (17)] and assuming a maximum under performance of 3σ for both maneuvers, a reduction value of $p = 0.0732231$ m/s is determined. A first Monte Carlo simulation was executed without including the effect of differential drag in order to verify if the final relative semi-major axis $a\delta a$ can assume a positive value, which would result in the satellites drifting towards each other. As can be seen in Figure 4, in none of the cases $a\delta a$ is positive. In the following figures, each dot represents one sample of the simulation. In Figures 4, 5 and 6, the remaining relative semi-major axis after the second maneuver is plotted against the mean separation in tangential direction. The left plots show the situation directly after the second maneuver, while the right ones show the development 24 hours later, when the third maneuver is about to be performed. The bold lines at $a\delta\lambda = 5000$ m and $a\delta\lambda = 10000$ m show the thresholds of separability by radar tracking and of visibility by the BIROS onboard camera.

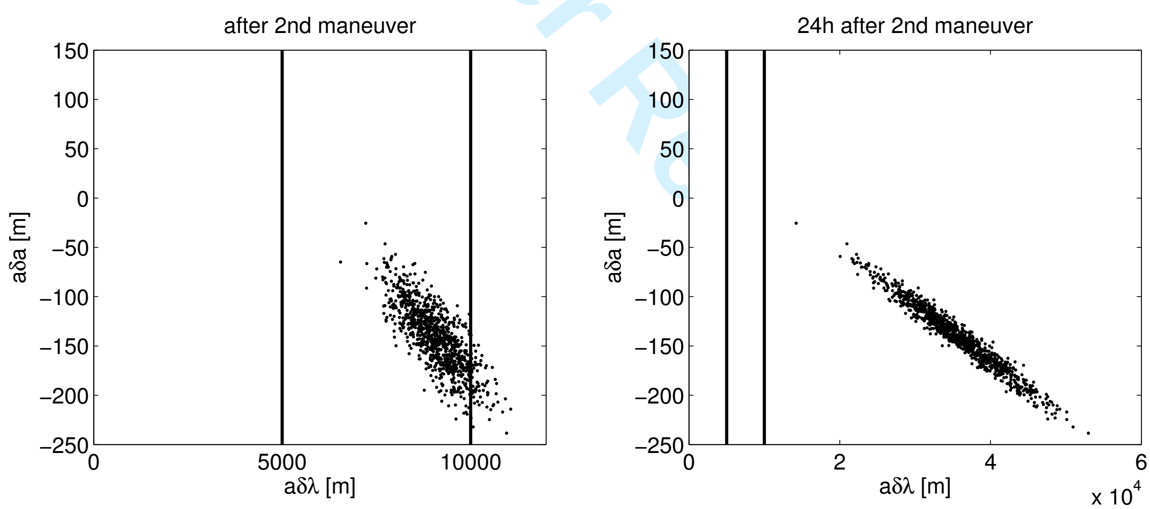

Figure 4. Residual $a\delta a$ in dependence of mean tangential separation ($p = 0.0732231$ m/s, no differential drag).

A second simulation run was executed with the differential drag effect taken into account and the reduction value p set to 0 in order to demonstrate the effect of the differential ballistic coefficient on the remaining drift. As can be see in Figure 5, in more than 40% of the cases $a\delta a$ is positive. In about 3.6 % of the cases, the drift induced by the relative semi-major axis has led to a reduction of the mean tangential separation to less than 5000 m and in 0.3 % of the cases the BIROS satellite even passed the picosatellite in tangential direction. This undesired approach leads to the two spacecraft being indistinguishable by radar tracking and renders relative orbit determination impossible.

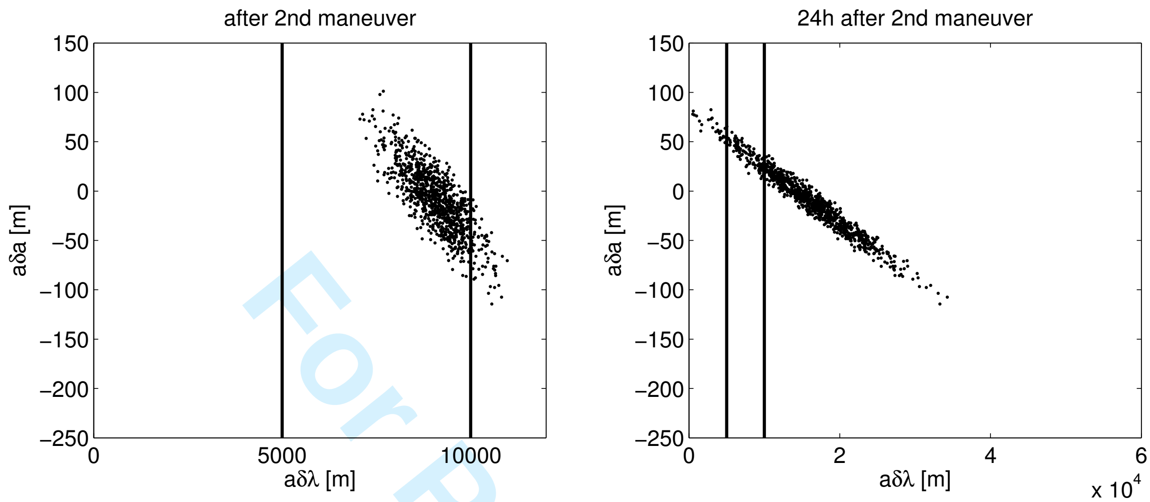

Figure 5. Residual $a\delta a$ in dependence of mean tangential separation ($p = 0$ m/s, drag included).

This demonstrates that the differential drag effect alone is not enough to prevent an approach of the satellites and a reduction of the tangential component of the second maneuver is necessary. The parameter p has to be tuned such that the likelihood of an approach of the satellites (i.e. $a\delta a > 0$), as well as that of an evaporation of the formation is minimized. A threshold of 50 km is defined as formation evaporation, since below that distance the formation can be recovered without too much effort from ground. Table 3 shows the probabilities of an approaching drift and formation evaporation for a selected range of p. The probability is computed by the number of events ($a\delta a > 0$ or $a\delta\lambda > 50$ km) divided by the total number of simulation runs. It is not possible to eliminate both the risks, but with a value of $p = 0.055$ m/s a minimum of the combined risk is found.

Table 3. Selection of the reduction value p for the nominal guidance plan of Eq. (17).

p [m/s]	$a\delta a > 0$ m	$a\delta\lambda > 50$ km
0.00	41.76 %	<0.01 %
0.01	22.59 %	<0.01 %
0.02	9.53 %	<0.01 %
0.03	3.16 %	<0.01 %
0.04	0.83 %	<0.01 %
0.05	0.17 %	0.01 %
0.055	0.07 %	0.03 %
0.06	0.03 %	0.08 %
0.07	0.01 %	0.36 %
0.08	<0.01 %	1.31 %

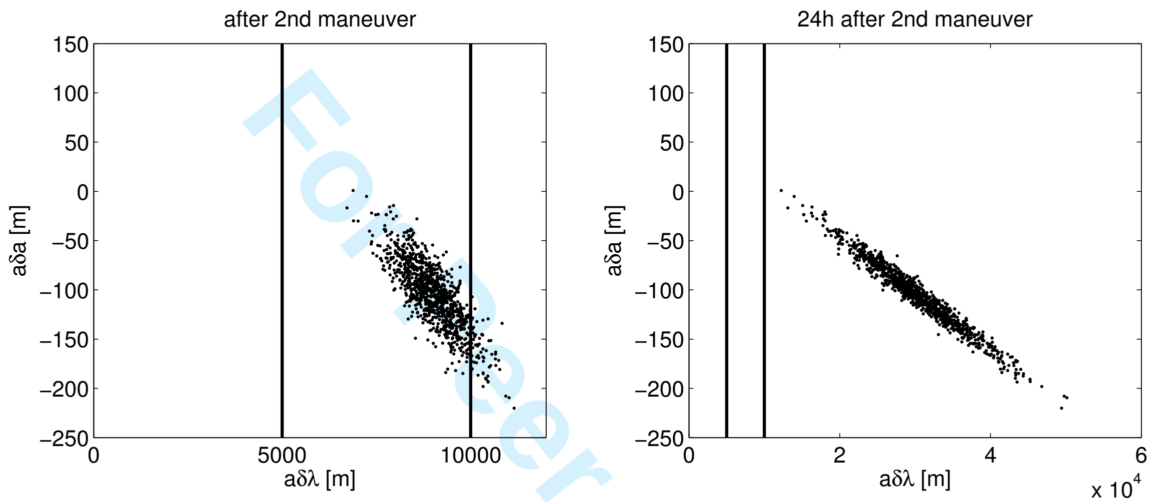

Figure 6. Residual $a\delta a$ in dependence of tangential separation ($p = 0.055$ m/s, drag included).

As stated above, a close approach of the satellites cannot be excluded with $p = 0.055$ m/s. This is confirmed by Figure 6, which shows that a very small number of cases with $a\delta a > 0$ remains. Hence, it needs to be verified that the established passive safety is sufficient to avoid a collision in case of an approach of the two spacecraft in tangential direction. The magnitudes of the relative eccentricity $a\delta e$ and relative inclination $a\delta i$ are shown in Figure 7. The limits for safety (150 m in both R and N) and visibility (596 m in R, 805 m in N) are indicated in the plot. It can be seen that in rare (0.02 %) cases the limits for visibility are violated, but the requirement on the minimum magnitude is always fulfilled.

In order to verify the passive safety, this magnitude information has to be complemented with the phasing of the relative e/i vectors. This allows to compute the minimum distance in the plane identified by R and N. Under the assumption of $a\delta a = 0$, the minimum separation perpendicular to

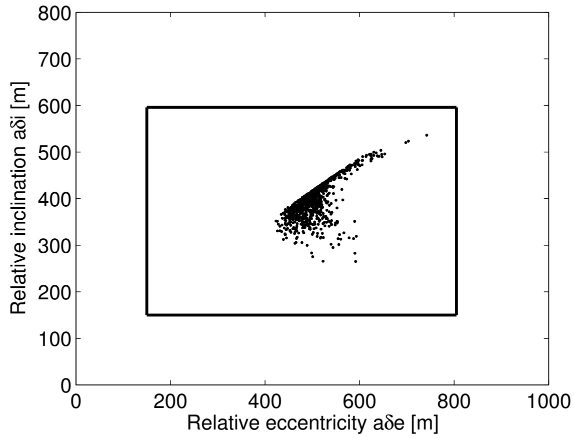

Figure 7. Relative eccentricity $a\delta e$ and inclination $a\delta i$ after 2nd maneuver.

the flight direction is defined as [10]:

$$\delta r_{nr}^{\min} = \frac{\sqrt{2}a\left|\delta\boldsymbol{e}\cdot\delta\boldsymbol{i}\right|}{\left(\delta e^2+\delta i^2+\left|\delta\boldsymbol{e}+\delta\boldsymbol{i}\right|\cdot\left|\delta\boldsymbol{e}-\delta\boldsymbol{i}\right|\right)^{1/2}} \tag{26}$$

This equation shows the importance of parallel or anti-parallel relative eccentricity and inclination vectors due to the scalar product of those vectors. In Figure 8 the minimum cross-track distance is plotted as a function of the residual $a\delta a$. As stated above, Eq.(26) is valid for $a\delta a = 0$, but in most cases $a\delta a$ is negative, thus the picosatellite is drifting towards greater separations. Only in the rare event of severe under-performance of the release mechanism, $a\delta a$ is close to 0. In these cases, $\delta r_{nr}^{\min}$ is about 150 m (see Figure 8), which means, that the passive safety of the formation is guaranteed.

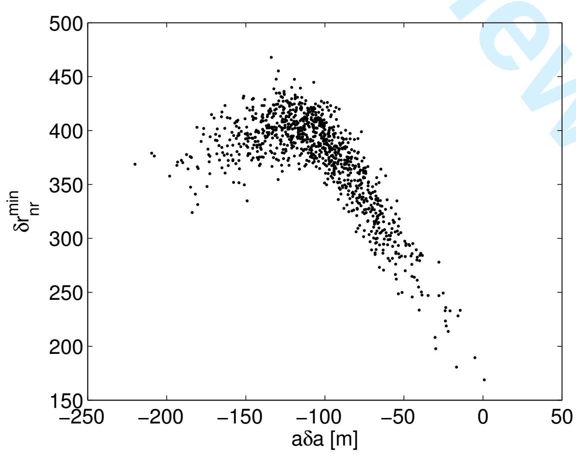

Figure 8. Minimum cross-track distance as a function of the final $a\delta a$.

Finally, it has to be verified, that a collision risk before the execution of the second maneuver can be ruled out. In case of a severe under-performance of the spring mechanism, the two spacecraft could approach after one revolution if not enough tangential separation has been built up. Therefore the tangential separation at the nearest crossing of the T–N plane is examined. Figure 9 shows that distance as a function of the performance factor f_1 of the separation mechanism. It can be seen that the behavior is almost linear, but even in the case of a 3σ under-performance ($f_1 < 0.7$), the tangential separation is still larger than 1600 m and no collision risk exists.

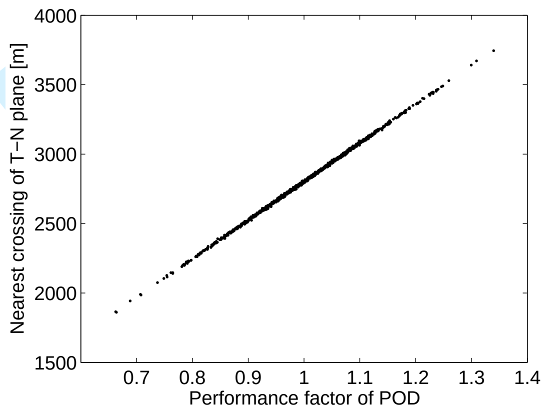

Figure 9. Nearest crossing of the T-N plane.

To conclude, the results of the robustness analysis of the baseline of Eq. (17) with the second tangential impulse reduced by a factor $p = 0.055$ m/s demonstrate that all the safety requirements are met, despite the uncertainties taken into account. At completion of the second maneuver, in fact, the residual relative semi-major axis is not positive with a mean along-track separation suitable for radar tracking observations (i.e., Figure 6), passive safety is guaranteed by always acceptable values of the minimum separation in the R–N plane (i.e., Figure 8), and the first cross through the $\mathrm{R} = 0$ axis happens at a definitely safe along-track separation (i.e., Figure 9). Therefore, after the picosatellite orbit determination is performed on-ground through radar tracking measurements, the initial conditions of the AVANTI experiment can be achieved by slowly drifting towards the picosatellite, without the need to substantially correct both relative eccentricity and inclination vectors.

The structure of the maneuvering scheme of Eq. (17) derives from the assumptions made in the preliminary design section. Since this study addresses an open-loop scheme, a minimum number of pre-computed pulses is planned and a consistent radial maneuver has to be performed at the expense of the thruster system of BIROS. Alternative baselines can be searched by allowing the separation to involve more maneuvers. In this case, in fact, the constraints affecting the final conditions would become active only after the execution of the last maneuver. This topic has to be investigated in the attempt to reduce the size of each single maneuver, and possibly, the overall delta-v consumption.

CONCLUSION

This paper addresses the design and the consequent feasibility analysis of the in-orbit release of a picosatellite from a small satellite carrier in low Earth orbit. This research embodies the prerequisite to the execution of the Autonomous Vision Approach Navigation and Target Identification experiment, scheduled for 2016. To this aim, a comprehensive overview of the mission requirements and of the operational aspects relevant to the mission safety are provided.

The peculiar scenario of aiming at a mid-range stable formation while employing a release mechanism that provides a large and strongly uncertain separation delta-v, demands the adaption of a well-known passive safety concept, based on the relative eccentricity/inclination vector separation, to cope with operational constraints and feasibility criteria. Specifically, the first one concerns the achievement of the minimum along-track separation to exploit a radar tracking campaign to perform relative orbit determination. Within this scenario, in fact, this represents the only available source of navigation information. The second criterion, closely related to the first one, asks the unavoidable residual drift to increase the relative separation, regardless of the magnitude and of the nature of the system's uncertainties. Finally, the last feasibility criterion is to reduce at minimum the probability of a formation evaporation, thus posing a condition in contrast with the first two.

This paper proposes a formalization of all these aforementioned safety requirements that allows addressing them already at the design level. This is accomplished by exploiting the powerful framework of the relative orbital elements. Moreover, this study supports the theoretical investigation through a numerical analysis which includes several sources of uncertainty, representative of the behavior of the space segment. As a result, a realistic assessment has been obtained which minimizes both collision and evaporation risks.

This research focuses on a double-impulse guidance strategy, where the first maneuver is provided by the deployment mechanism, whereas the second one is accomplished by the thrusters' system of the carrier satellite. Nevertheless, prior to the ultimate selection of the final mission plan, an analysis of the realistic performance of a multi-impulse separation scheme will be accomplished as well. According to the carrier thrusters' system, the involvement of a larger number of maneuvers allows distributing the needed delta-v over more but smaller burns. At a planning level, a larger range of relative configurations can be exploited in the intermediate phases, since only the final relative orbit is subjected to the complete set of constraints. The introduction of additional maneuvers can lead to a larger delta-v consumption. An increased number of maneuvers allows establishing the final relative orbit by firing the thrusters only in the tangential direction. This last point is beneficial to an overall reduction of the delta-v consumption.

REFERENCES

[1] H. Reile, E. Lorenz, and T. Terzibaschian, "The FireBird Mission - A Scientific Mission for Earth Observation and Hot Spot Detection," *Small Satellites for Earth Observation, Digest of the 9th International Symposium of the International Academy of Astronautics*, Berlin, Germany, Wissenschaft und Technik Verlag, 2013. ISBN 978-3-89685-574-9.

[2] B. Engberg, J. Ota, and J. Suchman, "The OPAL Satellite Project: Continuing the Next Generation Small Satellite Development," *Proceedings of the 9th Annual AIAA/US Conference on Small Satellites*, Logan, Utah, USA, 1995.

[3] J. Puig-Suari, C. Turner, and W. Ahlgren, "Development of the standard CubeSat deployer and a CubeSat class PicoSatellite," *Aerospace Conference, 2001, IEEE Proceedings*, Vol. 1, 2001, pp. 347–353, 10.1109/AERO.2001.931726.

[4] P. G. Ballard, A. Meza, S. Ritterhouse, T. Schaffer, C. Conley, C. Taylor, D. D. D. Atkine, and J. C. McLeroy, "Small Satellite Deployments From STS116 - Development Of New Manned Spaceflight Deployment Systems," *Proceedings of the AIAA/USU Conference on Small Satellites, Technical Session III: Launch & Propulsion Systems*, 2007, http://digitalcommons.usu.edu/smallsat/2007/all2007/19/.

[5] J. C. Springmann, A. Bertino-Reibstein, and J. W. Cutler, "Investigation of the on-orbit conjunction between the MCubed and HRBE CubeSats," *Aerospace Conference, 2013 IEEE*, 2013, pp. 1–8, 10.1109/AERO.2013.6497127.

[6] "Poly Picosatellite Orbital Deployer Mk III ICD," tech. rep., The CubeSat Program Std., 2007, http://cubesat.org/images/LaunchProviders/.

[7] P. Bodin, R. Noteborn, R. Larsson, T. Karlsson, S. D'Amico, J. S. Ardaens, M. Delpech, and J. C. Berges, "Prisma Formation Flying Demonstrator: Overview and Conclusions from the Nominal Mission," No. 12-072, Breckenridge, Colorado, USA, 35th Annual AAS Guidance and Control Conference, 2012.

[8] S. Persson, S. D'Amico, and J. Harr, "Flight Results from PRISMA Formation Flying and Rendezvous Demonstration Mission," Prague, Czech Republic, 61st International Astronautical Congress, 2010.

[9] S. D'Amico, O. Montenbruck, R. Larsson, and C. Chasset, "GPS-Based Relative Navigation during the Separation Sequence of the PRISMA Mission," No. AIAA-2008-6661, Honolulu, Hawaii, USA, AIAA Guidance, Navigation and Control Conference, 2008.

[10] S. D'Amico, *Autonomous Formation Flying in Low Earth Orbit*. PhD thesis, Technical University of Delft, The Netherlands, Mar. 2010.

[11] A. Härting, C. K. Rajasingh, M. C. Eckstein, A. F. Leibold, and K. N. Srinivasamurthy, "On the collision hazard of colocated geostationary satellites," No. 88-4239, Minneapolis, USA, AIAA/AAS Astrodynamics conference, 1988.

[12] O. Montenbruck, M. Kirschner, S. D'Amico, and S. Bettadpur, "E/I-Vector Separation for Safe Switching of the GRACE Formation," *Aerospace Science and Technology*, Vol. 10, No. 7, 2006, pp. 628–635. doi: 10.1016/j.ast.2006.04.001.

[13] S. D'Amico and O. Montenbruck, "Proximity Operations of Formation Flying Spacecraft using an Eccentricity/Inclination Vector Separation," *Journal of Guidance, Control and Dynamics*, Vol. 29, No. 3, 2006, pp. 554–563. doi: 10.2514/1.15114.

[14] J. Spurmann and S. D'Amico, "Proximity Operations of On-Orbit Servicing Spacecraft using an Eccentricity/Inclination Vector Separation," Sao Jose dos Campos, Brazil, 22nd International Symposium on Spaceflight Dynamics, 2011.

[15] G. Gaias and S. D'Amico, "Impulsive Maneuvers for Formation Reconfiguration using Relative Orbital Elements," *Journal of Guidance, Control, and Dynamics*, 2014. accessed April 22 2014, doi: 10.2514/1.G000189.

[16] G. Gaias, J.-S. Ardaens, and S. D'Amico, "The Autonomous Vision Approach Navigation and Target Identification (AVANTI) Experiment: Objectives and Design," Porto, Portugal, 9th International ESA Conference on Guidance, Navigation & Control Systems, 2014.

[17] J.-S. Ardaens and G. Gaias, "Spaceborne Autonomous Vision-Based Navigation System for AVANTI," Toronto, Canada, 65th International Astronautical Congress, 2014.

[18] T. Karlsson, N. Ahlgren, R. Faller, and B. Schlepp, "PRISMA Mission Control: Transferring Satellite Control between Organisations," Stockholm, Sweden, SpaceOps 2012, 2012.

[19] R. Kahle, M. Weigel, M. Kirschner, S. Spiridonova, E. Kahr, and K. Letsch, "Relative Navigation to Non-cooperative Targets in LEO: Achievable Accuracy from Radar Tracking Measurements," *International Journal of Space Science and Engineering*, Vol. 2, No. 1, 2014, pp. 81–95.

[20] S. D'Amico, J.-S. Ardaens, G. Gaias, H. Benninghoff, B. Schlepp, and J. L. Jørgensen, "Noncooperative Rendezvous Using Angles-Only Optical Navigation: System Design and Flight Results," *Journal of Guidance, Control, and Dynamics*, Vol. 36, No. 6, 2013, pp. 1576–1595. doi: 10.2514/1.59236.

[21] W. H. Clohessy and R. S. Wiltshire, "Terminal Guidance System for Satellite Rendezvous," *Journal of the Aerospace Sciences*, Vol. 27, No. 9, 1960, pp. 653–658.

[22] S. D'Amico, "Relative Orbital Elements as Integration Constants of Hill's Equations," DLR-GSOC TN 05-08, Deutsches Zentrum für Luft- und Raumfahrt, Oberpfaffenhofen, Germany, Dec. 2005.